Neutral helium spectral lines in dense plasmas

Banaz Omar,[1] Sibylle Günter,[2] August Wierling,[1] and Gerd Röpke[1]
[1]*Universität Rostock, Institut für Physik, 18051 Rostock, Germany*
[2]*Max-Planck-Institut für Plasmaphysik, 85748 Garching, Germany*
(Received 21 October 2005; revised manuscript received 3 January 2006; published 24 May 2006)

Shift and broadening of isolated neutral helium lines 7281 Å (2^1P-3^1S), 7065 Å (2^3P-3^3S), 6678 Å (2^1P-3^1D), 5048 Å (2^1P-4^1S), 4922 Å (2^1P-4^1D), and 4713 Å (2^3P-4^3S) in a dense plasma are investigated. Based on a quantum statistical theory, the electronic contributions to the shift and width are considered, using the method of thermodynamic Green functions. Dynamic screening of the electron-atom interaction is included. Compared to the width, the electronic shift is more affected by dynamical screening. This effect increases at high density. A cut-off procedure for strong collisions is used. The contribution of the ions is taken into account in a quasi-static approximation, with both the quadratic Stark effect and the quadrupole interaction included. The results for shift and width agree well with the available experimental and theoretical data.

DOI: 10.1103/PhysRevE.73.056405 PACS number(s): 52.70.−m, 32.70.Jz

I. INTRODUCTION

Line profile calculations are an interesting tool for both laboratory and astrophysical plasmas, e.g., to determine the internal parameters or to understand the microscopic processes within the plasma [1,2]. Helium spectral lines can be used for diagnostics of laboratory plasmas, such as shock wave tube or pulsed arc plasmas [3–6], and in the astrophysical context of stellar atmospheres of hot stars and white dwarfs [7–10]. The 7065 Å line is used in radiative transfer calculations for supernovae [11,12] and cataclysmic variables [13]. The 6678 Å line is of importance to determine physical properties of massive compact binaries [14]. The line 4713 Å is a dominant one in helium-rich hot subdwarfs [15]. The line 7281 Å is observed in P Cyg [16]. The two lines 5048 Å and 4713 Å appear in the spectrum of CI Cam (sgB[e] star), and they are less optically thick than most of the helium lines in the spectrum [17]. Furthermore, He-like spectral lines are a prominent feature in laser-generated plasmas [18–22]. In addition to this, a detailed analysis of the broadening and shift of helium spectral lines of dense plasmas can be used to test our understanding of correlation effects in these plasmas [23,24].

A review of recent experimental data for Stark broadening of nonhydrogenic neutral atoms is given by Konjević *et al.* [25,26]. In particular, Refs. [3–7,21,22,27–32] concern the lines studied in this paper. Stark broadening of several isolated neutral helium lines, such as 7281 Å, 7056 Å, 6678 Å, 5016 Å, 4713 Å, and 3889 Å, emitted from dense plasmas have been measured in a low-pressure pulsed arc plasma by Pérez *et al.* [3–5]. In these experiments, the electron density was determined by interferometry for different wavelengths, and the plasma electron temperature was estimated from a Boltzmann plot or the intensity ratio of the ion and neutral lines. Stark shift of the He I lines 3889 Å, 5016 Å, 7281 Å, and 6678 Å have been measured by Djeniže *et al.* [28] in a linear pulsed arc plasma, using a shot-by-shot technique. Further experiments are reported for the He I in Refs. [18,33–46], such as the Stark profile measurement of the He I at 5876 Å performed by Büscher *et al.* [34] for an electron density in the range of $N_e=(0.5-2.5)\times 10^{18}$ m^{-3} and a temperature of $T=(4-5.5)$eV. Deviation from a linear density dependency of Stark broadening parameters has been observed. Profiles of the He I 4471 Å and 4922 Å spectral lines were measured by Frank *et al.* [35]. The relatively weak forbidden components appear on the wing of the corresponding allowed transitions. Both mentioned transitions are investigated by Adler and Piel [36] at low electron densities ranging from $N_e=(10^{20}-10^{21})$m^{-3}.

To calculate the line profile in dense plasmas on a microscopic level, modifications due to the surrounding particles must be taken into account. Screening as an important collective effect in a plasma has to be considered. Note that the influence of electrons and ions can be treated separately due to the difference in mass and mobility. Various approaches have been modified to account these effects [47–52]. Helium series were calculated from a semiclassical approach by Griem *et al.* [51,52], using a traditional impact approximation for electrons with a cut-off procedure, while almost-stationary heavy ions are treated in a quasi-static ion approximation due to the static microfield.

At low electron densities, moving ions cause a considerable change in the value and the direction of the electric field. This leads to additional broadening of spectral lines which is not taken into account by a static ion microfield [53]. Note also that the dynamical treatment of ions is important for overlapping lines. The influence of the motion of the perturbing ions on the Stark line shapes can be considered, e.g., within the model microfield method (MMM) [54] or by molecular dynamics simulations of the line profiles [23]. Molecular dynamics (MD) simulations have been performed by Gigosos *et al.* [23,55], by introducing two kinds of simulations for calculating He I Stark line profiles. At relatively high electric fields, the mixing of different sublevels for transitions involving highly excited states leads to forbidden transitions and the increasing importance of the linear Stark effect [8].

Recently, a quantum statistical many-body approach taking into account the medium effects by using thermodynamic Green function technique has been developed [56,57]. In

principle, this approach is able to describe dynamical screening and strong collisions by electrons, as well as the dynamic ion microfield in a systematic way. In contrast to molecular dynamics simulations, a consistent quantum description is performed. It has been successfully applied to Lyman and Balmer lines of dense hydrogen plasmas [58–60]. In this work, the Green function approach to spectral line shapes of nonideal plasmas is extended to helium lines. A review of the basic formalism is presented in Sec. II. In Sec. III, the shift and full width at half maximum (FWHM) for isolated nonoverlapping He I lines 7281 Å, 7065 Å, 6678 Å, 5048 Å, and 4713 Å, and the electronic contributions of line 4922 Å, are evaluated and discussed. Results for the shift and broadening are compared with a number of recent experiments and theoretical calculations. Finally, conclusions are given in Sec. IV.

II. THEORY OF SPECTRAL LINES IN DENSE PLASMAS

A quantum statistical approach has been developed to account, in a systematic way, for medium modifications of spectral line shapes [56,61,62]. It starts from the relation of the absorption coefficient $\alpha(\omega)$ and the refraction index $n(\omega)$ to the dielectric function $\epsilon(\mathbf{q},\omega)$ in the long wavelength limit $q\to 0$,

$$\alpha(\omega)=\frac{\omega}{cn(\omega)}\lim_{q\to 0}\mathrm{Im}\,\varepsilon(\mathbf{q},\omega), \tag{1}$$

$$n(\omega)=\frac{1}{\sqrt{2}}\lim_{q\to 0}\Big\{\mathrm{Re}\,\varepsilon(\mathbf{q},\omega)+\big[(\mathrm{Re}\,\varepsilon(\mathbf{q},\omega))^2+(\mathrm{Im}\,\varepsilon(\mathbf{q},\omega))^2\big]^{1/2}\Big\}^{1/2}. \tag{2}$$

The dielectric function can be determined from the polarization function $\Pi(\mathbf{q},\omega)$ according to $\epsilon(\mathbf{q},\omega)=1-V(q)\Pi(\mathbf{q},\omega)$, where $V(q)=e^2/(\epsilon_0\Omega_0 q^2)$ is the Fourier transformed Coulomb potential. Using thermodynamic Green functions, a systematic perturbative treatment of the polarization function can be performed.

The polarization function $\Pi(\mathbf{q},\omega)$ is related to the dipole-dipole autocorrelation function [57]. The following expression for the full profile $I(\omega)$ is obtained as a convolution of the Doppler-broadened line profile with the pressure-broadened line profile $I^{\mathrm{pr}}(\omega)$:

$$I(\omega)\sim\int_{-\infty}^{\infty}\frac{d\omega'}{\omega'}\exp\left[-\frac{m_i c^2}{2k_{\mathrm{B}}T}\left(\frac{\omega-\omega'}{\omega'}\right)^2\right]I^{\mathrm{pr}}(\omega'), \tag{3}$$

where m_i is the mass of the radiating atom and c is the speed of light. The perturber-radiator interaction leads to a pressure broadening (Stark broadening), which contains an electronic and an ionic contribution. Describing the ionic contribution in the quasi-static approximation by averaging over the ionic microfield [47,57,63], we get

$$I^{\mathrm{pr}}(\omega)\sim\sum_{i,i',f,f'}I_{i,i'}^{f,f'}(\omega)\int_0^{\infty}d\beta P(\beta)\mathrm{Im}\langle i|\langle f|\left[\hbar\omega-\hbar\,\omega_{if}-\Sigma_{if}(\omega,\beta)+\mathrm{i}\Gamma_{if}^{\mathrm{V}}\right]^{-1}|f'\rangle|i'\rangle. \tag{4}$$

Here, $\hbar\omega_{if}=E_i-E_f$ is the unperturbed transition frequency between the initial i and the final f states, i' and f' are the corresponding intermediate states

$$I_{i,i'}^{f,f'}(\omega)=\langle i|\mathbf{r}|f\rangle\langle f'|\mathbf{r}|i'\rangle\frac{\omega^4}{8\pi^3c^3}\mathrm{e}^{-\hbar\omega/k_{\mathrm{B}}T}, \tag{5}$$

where $\langle i|\mathbf{r}|f\rangle$ has to identified as a dipole matrix element for the transition between i and f states. The ionic microfield $P(\beta)$ is taken according to the Hooper microfield distribution and $\beta=E/E_0$ is the normalized microfield strength at ion density $N_i=N_e$ with Holtsmark normal field strength $E_0=e/(4\pi\epsilon_0 r_0^2)$, where $\frac{4}{15}(2\pi)^{3/2}r_0^3N_i=1$ [64]. The line profile itself is determined by the vertex correction Γ_{if}^{V} for the overlapping lines and the self-energy corrections of the initial Σ_i and final states Σ_f,

$$\Sigma_{if}(\omega,\beta)=\mathrm{Re}\big[\Sigma_i(\omega,\beta)-\Sigma_f(\omega,\beta)\big]+\mathrm{i}\,\mathrm{Im}\big[\Sigma_i(\omega,\beta)+\Sigma_f(\omega,\beta)\big]. \tag{6}$$

Electronic, as well as ionic, contributions occur in the self-energy $\Sigma_n(\omega,\beta)$, which is assumed to be diagonal in the atomic state n,

$$\Sigma_n(\omega,\beta)=\Sigma_n^{\mathrm{ion}}(\beta)+\Sigma_n^{\mathrm{el}}(\omega,\beta). \tag{7}$$

We describe expressions to calculate the self-energy and vertex contributions. Performing a Born approximation with respect to the perturber-radiator interaction, the electronic self-energy is obtained as [57]

$$\Delta_n^{\mathrm{SE}}+\mathrm{i}\Gamma_n^{\mathrm{SE}}=\langle n|\Sigma^{\mathrm{el}}(E_n,\beta)|n\rangle=-\frac{1}{e^2}\int\frac{\mathrm{d}^3q}{(2\pi)^3}V(q)\sum_{\alpha}|M_{n\alpha}(\mathbf{q})|^2\times\int_{-\infty}^{\infty}\frac{\mathrm{d}\omega}{\pi}[1+n_B(\omega)]\frac{\mathrm{Im}\,\varepsilon^{-1}(\mathbf{q},\omega+\mathrm{i}0)}{E_n-E_\alpha(\beta)-(\omega+\mathrm{i}0)}. \tag{8}$$

Here, the level splitting due to the ion microfield has been neglected [65], $n_{\mathrm{B}}(\omega)=[\exp(\hbar\omega/k_{\mathrm{B}}T)-1]^{-1}$ is the Bose distribution function and $M_{n\alpha}(\mathbf{q})$ are the transition matrix elements given below. The sum over α runs from $n-1$ to $n+1$ discrete bound states for virtual transitions. The inverse dielectric function $\varepsilon^{-1}(\mathbf{q},\omega)$ contains many particle effects which account for the dynamical screening of the interaction in the plasma

$$\mathrm{Im}\,\varepsilon^{-1}(\mathbf{q},\omega)=-\frac{\mathrm{Im}\,\varepsilon(\mathbf{q},\omega)}{[\mathrm{Re}\,\varepsilon(\mathbf{q},\omega)]^2+[\mathrm{Im}\,\varepsilon(\mathbf{q},\omega)]^2}. \tag{9}$$

The random phase approximation (RPA) for the dielectric function is used

$$\varepsilon^{\mathrm{RPA}}(\mathbf{q},\omega) = 1 - 2V(q)\int \frac{d^3p}{(2\pi)^3}\frac{f_e(E_\mathbf{p}) - f_e(E_{\mathbf{p}+\mathbf{q}})}{E_\mathbf{p} - E_{\mathbf{p}+\mathbf{q}} - \hbar\,(\omega + \mathrm{i}0)}, \tag{10}$$

where $E_\mathbf{p}=\hbar^2\mathbf{p}^2/2m_e$ is the kinetic energy of electrons and $f_e(E_\mathbf{p})$ is the Fermi distribution function of the electrons

$$f_e(E_\mathbf{p}) \simeq \frac{1}{2}N_e\left(\frac{2\pi\hbar^2}{m_e k_\mathrm{B}T}\right)^{3/2}\exp\left(-\frac{\hbar^2p^2}{2m_e k_\mathrm{B}T}\right). \tag{11}$$

The full expression of the inverse dielectric function has to be used if the transition frequency $\omega_{n\alpha}$ becomes comparable to the electron plasma frequency $\omega_\mathrm{pl}=(N_e e^2/\epsilon_0 m_e)^{1/2}$. However, in the high-frequency limit $\omega_{n\alpha} \gg \omega_\mathrm{pl}$, the inverse dielectric function can be approximated by

$$\mathrm{Im}\ \varepsilon^{-1}(\mathbf{q},\omega) \approx -\mathrm{Im}\ \varepsilon(\mathbf{q},\omega). \tag{12}$$

This binary collision approximation leads to a linear behavior of the electronic shift contribution with respect to the electron density, whereas a nonlinear dependence of the electronic shift with increasing electron density is expected if the full expression of the inverse dielectric function is used [65,66]. For virtual transitions between states with the negligible energy difference, the static Debye screening can be considered for the inverse dielectric function such as [58,65]:

$$\mathrm{Im}\ \varepsilon^{-1}(\mathbf{q},0) = \frac{\mathrm{Im}\ \varepsilon(\mathbf{q},0)}{(1+\kappa^2/q^2)^2}, \tag{13}$$

where $\kappa=r_D^{-1}=[2e^2N_e/(\epsilon_0 k_B T)]^{1/2}$ is the inverse Debye radius. On the other hand, the static Debye screening can be also applied in the semiclassical calculation by using the cut-off parameter $\rho_\mathrm{max}=1.1r_D$, according to Griem [52]. In our case, the lower limit $q_\mathrm{min}=1/\rho_\mathrm{max}$ of the q-integration can be selected.

The vertex function for the coupling between the upper and the lower state is given by

$$\Gamma_{if}^V = \frac{2\pi}{e^2}\int \frac{d^3q}{(2\pi)^3}\frac{d^3p}{(2\pi)^3}f_e(E_\mathbf{p})V^2(q)M_{ii}(\mathbf{q}) \times M_{ff}(-\mathbf{q})\,\delta\left(\frac{\hbar^2\mathbf{p}\cdot\mathbf{q}}{m_e}\right). \tag{14}$$

The transition matrix elements $M_{n\alpha}(\mathbf{q})$ describe the coupling between free charges and bound states. In lowest order, they are determined by the atomic eigenfunctions $\psi_n(\mathbf{P})$ of the radiating electron and depend on the momentum transfer, $\hbar\mathbf{q}$ [56,61],

$$M_{n\alpha}(\mathbf{q}) = \int \frac{\mathrm{d}^3p}{(2\pi)^3}\psi_n^*(\mathbf{p})\left[Z_n e\psi_\alpha(\mathbf{p}) - e\psi_\alpha(\mathbf{p}+\mathbf{q})\right]$$

$$= ie\left(Z_n\delta_{n\alpha} - \int \mathrm{d}^3r\psi_n^*(\mathbf{r})\exp(\mathrm{i}\mathbf{q}\cdot\mathbf{r})\psi_\alpha(\mathbf{r})\right),$$

assuming $m_e \ll m_i$ and Z_n is the ion charge. Expanding the plane wave into spherical harmonics

$$\exp(\mathrm{i}\mathbf{q}\cdot\mathbf{r}) = 4\pi\sum_{l=0}^{\infty}\sum_{m=-l}^{l}\mathrm{i}^l j_l(qr)Y_{lm}^*(\Omega_q)Y_{lm}(\Omega_r), \tag{15}$$

a multipole expansion can be derived, e.g., $l=0,1,2$ gives the monopole, dipole, and quadrupole contribution of the radiator-electron interaction, respectively.

Contrary to hydrogen or hydrogenlike ions, the bound state wave functions are not explicitly known for helium. Approximations have to be made. Here, we assume for the spherical part of the wave function a linear combination of hydrogenlike wave functions, while the radial part of the matrix element in dipole transition is calculated based on the Coulomb approximation method of Bates and Damgaard [67–69]. In more detail, $P_{n,l}(r)$ is related to the normalized radial eigenfunctions of the jumping electron. A series expansion of these wave functions in terms of hydrogenic wave functions is considered:

$$P_{nl}(r) = rR_{nl}(r) = \left(\frac{2r}{n^*}\right)^{n^*}\exp\left(-\frac{r}{n^*}\right)\sum_{k=0}^{k_\mathrm{max}}\frac{a_k}{r^k}. \tag{16}$$

The effective principal quantum number n^* depends on the ionization energy of neutral helium and the energy of the corresponding state according to

$$n^* = \sqrt{\frac{1\mathrm{Ry}}{E_\infty - E_{nl}}},$$

$$a_k = a_{k-1}\frac{n^*[l(l+1) - (n^*-k)(n^*-k+1)]}{2k},$$

$$a_0 = 1/n^*[\Gamma(n^*+l+1)\Gamma(n^*-l)]^{1/2}. \tag{17}$$

To ensure convergence, the series should be truncated [68] by $a_k=0$ for $k_\mathrm{max}=k>n^*+0.5$.

As stated above, the electronic contribution of the self-energy is evaluated in the Born approximation. This overestimates the self-energy. In particular, strong collisions with large momentum transfer are not treated appropriately by the Born approximation, while the perturbation theory breaks down at small distances. A systematic calculation for strong collisions is possible by the partial summation of diagrams forming a three-particle T-matrix [57] or by using the close-coupling method [70]. To avoid a perturbative expansion with respect to the interaction, strong collision contributions to the broadening are estimated by a Lorentz–Weisskopf approximation [51,52,69] with the introduction of a cut-off parameter for the q-integration [see Eq. (8)]. Following Griem, this cut-off parameter is the inverse of the minimum limiting impact parameter ($q_\mathrm{max}=1/\rho_\mathrm{min}$) [57]

$$\rho_\mathrm{min} = \left[\frac{2\mathrm{e}^4}{3\hbar^2v^2}\sum_\alpha |\langle i|\mathbf{r}|\alpha\rangle|^2|A(z_{i\alpha}^\mathrm{min}) + iB(z_{i\alpha}^\mathrm{min})|\right]^{1/2},$$

$$z_{i\alpha}^\mathrm{min} = (E_i - E_\alpha)\rho_\mathrm{min}/\hbar\,v,$$

$$A(z) = z^2[K_0^2(|z|) + K_1^2(|z|)],$$

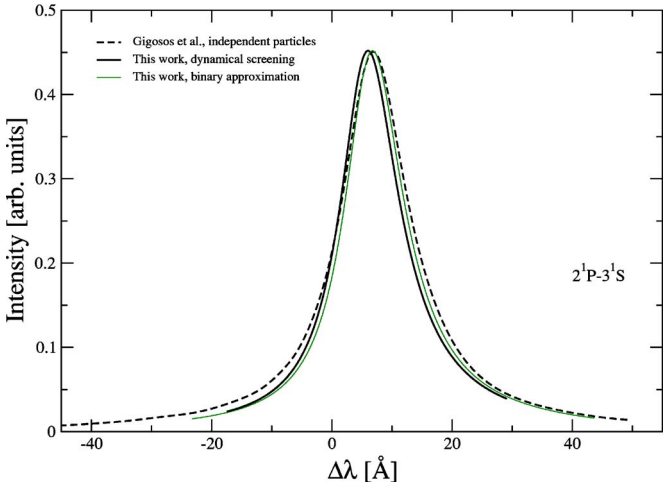

FIG. 1. (Color online) Theoretical spectral line profile (solid line) of He I line 7281 Å for an electron density of 1.457×10^{23} m^{-3} and a temperature of 2×10^4 K, compared with calculations of Gigosos *et al.* (broken line) [75].

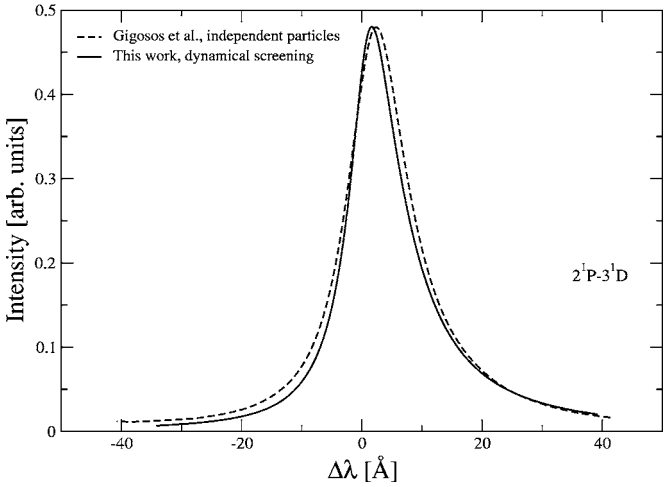

FIG. 2. Theoretical spectral line profile of He I line 6678 Å (solid line) for an electron density of 14.57×10^{22} m^{-3} and a temperature of 2×10^4 K, comparison is made with Gigosos *et al.* [75] (broken line).

$$B(z) = \pi z^2 [K_0(z) I_0(z) - K_1(z) I_1(z)], \tag{18}$$

where I and K are modified Bessel functions [52]. An appropriate strong electronic collision term for the width of neutral helium, which is also introduced by Griem *et al.* [51], should be added to the width in Eq. (8), and the shift according to Eq. (3.17) in Ref. [51] as follows:

$$\Delta^{\text{total}} = \Delta_n^{SE} + \left(\frac{3}{4}\right)^{2/3} N_e \int v \pi \rho_{\min}^2 f(v)\, dv, \tag{19}$$

with the Maxwellian velocity distribution function,

$$f(v) = 4\pi v^2 \left(\frac{m_e}{2\pi k_B T_e}\right)^{3/2} \exp\left(-\frac{m_e v^2}{2 k_B T_e}\right), \tag{20}$$

where v is electron velocity, and N_e is the electron density.

For the ionic contribution to the self-energy, we approximate the time-dependent microfield fluctuation by its static value. In general, the dynamic ionic microfield is important for overlapping lines and at low electron density in the line center [71,72]. Due to the slow movement of heavy ions, the ion microfield is assumed to be constant during the time of interest for the radiation process. The perturbing ions can be considered to be static during the radiation except in the line center. The static ionic contribution to the ionic self-energy is treated by means of the microfield concept including both quadratic Stark effect and quadrupole effects. The first-order perturbation term vanishes for nonhydrogeniclike atoms because of nondegeneracy with respect to the orbital quantum number l. According to second-order perturbation theory, the quadratic Stark effect is proportional to the square of the microfield [73]:

$$\Sigma_{nlm}^2(E) = e^2 |E|^2 \sum_{n',l',m'} \frac{|\langle n,l,m|z|n',l',m'\rangle|^2}{E_{nlm} - E_{n'l'm'}}, \tag{21}$$

where E is the microfield strength, n, l, and m are the well known principal, orbital, and magnetic atomic quantum numbers, respectively. The quadrupole Stark effect is due to the inhomogeneity of the ionic microfield. We use the expression derived by Halenka [74],

$$\Sigma_{nn'}^3(E) = -\frac{5}{2\sqrt{32\pi}} \frac{eE_0}{r_0} B_\rho(\beta) \langle n|3z^2 - r^2|n'\rangle.$$

Here, $B_\rho(\beta)$ is the mean field gradient at a given field strength, and the screening parameter $\rho = r_0/r_D$ is taken as the ratio between the mean particles distance r_0 [see below Eq. (5)] and the Debye radius r_D.

III. RESULTS

Applying the formalism outlined above, helium line profiles can be calculated for given electron densities and temperatures. From these profiles, a FWHM and a shift of the

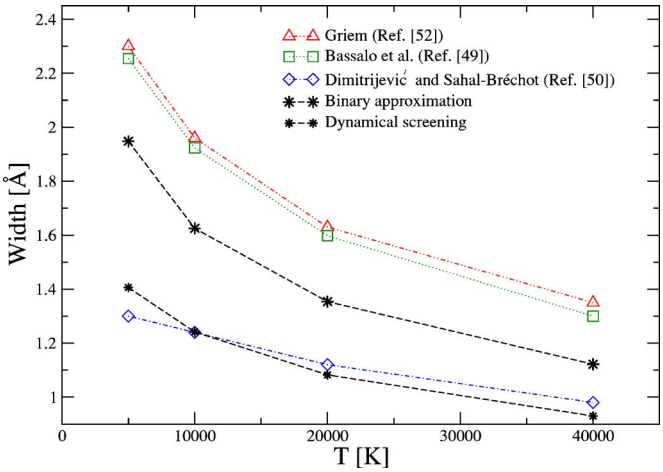

FIG. 3. (Color online) Electronic width HWHM of He I line 4922 Å for electron density 1.0×10^{22} m^{-3} as a function of temperature.

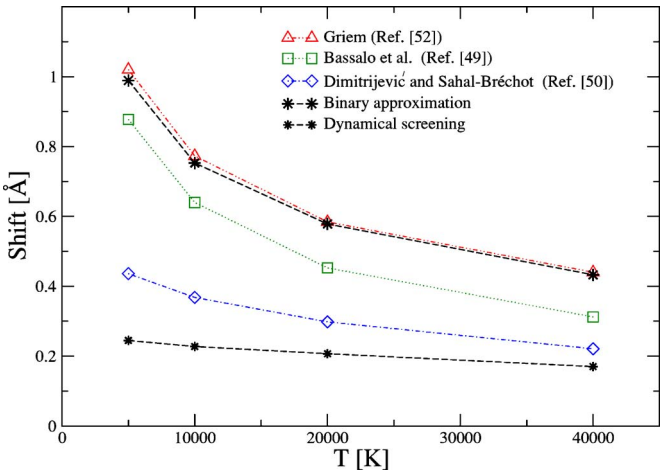

FIG. 4. (Color online) Electronic shift of He I line 4922 Å for electron density 1.0×10^{22} m^{-3} as a function of the temperature.

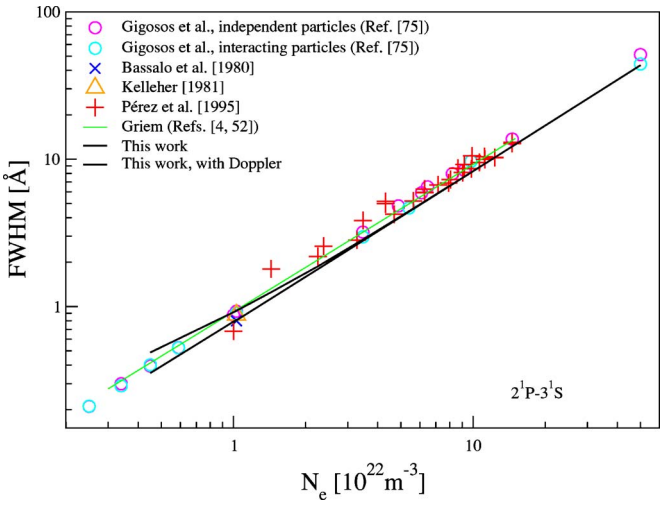

FIG. 5. (Color online) The FWHM for the He I line 7281 Å versus electron density. Comparison is made with available theoretical and experimental data. The electron temperature is taken according to references [4,30,75,76], see also Table III.

peak position can be determined; the value of the line shift is obtained from the distance between the unperturbed line and the peak position of the profile, while the full width of the profile is determined from the positions whose intensity are one-half of the intensity of the maximum of the line. Note that different expressions of shift, such as the shift of center of mass or the shift at half-width, exist [30]. Here, our definition follows the definitions used in the experimental studies.

We present results of the spectral line shapes of the isolated He I lines (2^1P-3^1S), (2^3P-3^3S), (2^1P-3^1D), (2^1P-4^1S), and (2^3P-4^3S). Also, the electronic shift and width for the transition (2^1P-4^1D) in dense plasmas are calculated. However, the profile of this line merges with its forbidden component [35,36]. The Born approximation—with respect to the dynamically screened electron-atom interaction—is given by Eq. (9), and a binary approximation has been considered—according to Eq. (12). As an example, we compare the spectral profile for the transitions 7281 Å (2^1P-3^1S) and 6678 Å (2^1P-3^1D) in Figs. 1 and 2 with simulation results obtained by Gigosos *et al.* [75]. As can be seen, a perfect agreement between our results in a binary approximation and the simulation data is found for the 7281 Å in the line center, small discrepancies arise in the line wings; while in the case of dynamical screening, the line shift becomes smaller. As for the 6678 Å line, although the discrepancy is somewhat larger, still the overall agreement is reasonable. The simulation result shown here is used only for independent particles. Comparison with the more realistic case of interacting particles would, of course, be more meaningful [75]. Note, that the asymmetry of the spectral line shape is small in the case of 7281 Å line but larger for the 6678 Å line.

In Figs. 3 and 4, we show the electronic width [half width at half maximum (HWHM)] and shift for the 4922 Å line, respectively, as a function of temperature at electron density $N_e=1.0\times10^{22}$ m^{-3}. Comparison is made with theoretical values given by Griem [52], Bassalo *et al.* (BCW) [49], and Dimitrijević and Sahal-Bréchot (DSB) [50]. In general, our results are similar in size to previous calculations, and the temperature dependence is similar as well. The binary approximation result for a shift delivers good agreement with the other calculations for this transition. In our calculation, the effect of dynamical Debye screening is considered which leads to reduction of electronic shift and width. In the standard theory of Griem [52], a semiclassical impact approach is used. The importance of the correction for Debye screening at high density was pointed out, especially, when the plasma frequency becomes larger than the splitting between interacting levels [1]. For this transition, the reduction of the width is about 20% in the given temperature range. An approximation for strong electron collisions is attended, in which the perturbation theory breaks down. The cut-off procedure has been developed and used extensively by Griem and collaborations [51,52,69], as well as in the semiclassical formalism by Dimitrijević and Sahal-Bréchot [50]. Bassalo *et al.* [49] assumed, in their calculations, the convergent method [68] in a many-level approximation.

Next, the total width and the total shift for the line 7281 Å as a function of the electron density are given in Figs. 5 and 6, respectively. Doppler broadening is included according to Eq. (3). We compare our results with the visible spectrum emitted by a helium plasma generated in a wall-stabilized arc, which is reported by Kelleher [30]. The determined electron density was 1.03×10^{22} m^{-3} at electron and gas temperatures of 2.09×10^4 K and 1.58×10^4 K, respectively. The semiclassical approach of Bassalo *et al.* [76] was assumed for Debye screening by introducing the Debye cut-off parameter. The broadening and shift due to electron collisions with and without the Debye screening effect were estimated. The ion contribution has been treated in the same way as in the approach developed by Griem [52]. The results obtained by a MD simulation for independent and interacting particles by Gigosos *et al.* [23,75] cover the density range of $(0.25-50.0)\times10^{22}$ m^{-3} and temperature range of $(1.9-4.2)\times10^4$ K, while for the values obtained in a pulse arc plasma by Pérez *et al.* [4] the temperature lies in the interval of

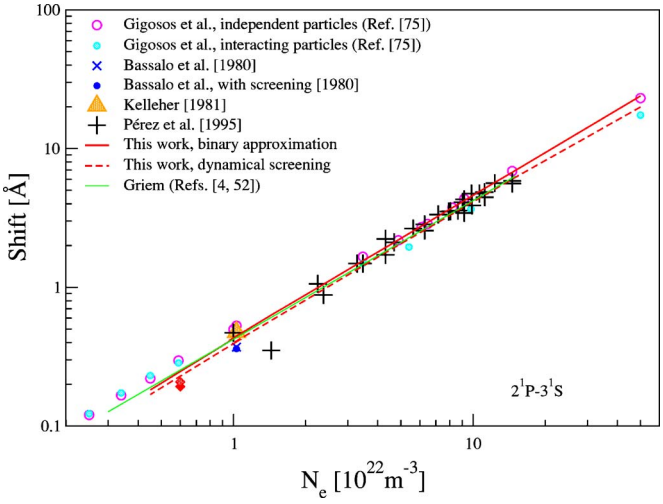

FIG. 6. (Color online) The shift of the He I line 7281 Å versus electron density. Comparison is made with available theoretical and experimental data. The electron temperature is taken according to the references [4,30,75,76], see also Table II.

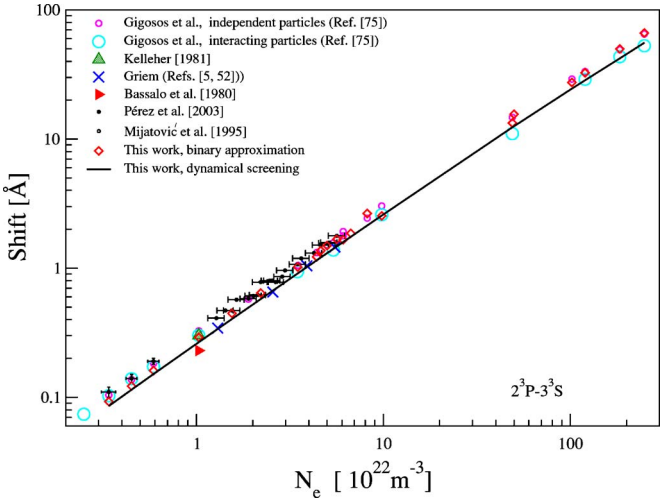

FIG. 7. (Color online) The shift of the He I line 7065 Å versus electron density. Comparison is made with available theoretical and experimental data. The electron temperature is taken according to the references [5,27,30,32,52,75,76], see also Tables II and IV.

$(1.6-2.5)\times10^4$ K with a mean value around 2×10^4 K. They included the estimated theoretical data from Griem approach [52]. In the calculation of Gigosos *et al.* [75], no Doppler broadening is taken into account.

The overall agreement of our result with results from other authors is quite good. In comparison to the estimated values of Griem [4,52], the deviations are more pronounced for the width than for the shift. The discrepancies are larger at very low density. At lower densities, the Stark broadening becomes less important, and the relative contribution of Doppler broadening increases. However, ion dynamics—which is not considered in this paper—becomes important at low densities. This might be the reason for the discrepancies at very low densities.

Our results for shift and FWHM versus electron density for the transition 7065 Å are given in Figs. 7 and 8, respectively. Comparisons are made with: (i) A number of measured [30,32,77] and theoretical data [76], (ii) observation in a repetitively pulsed low-pressure arc hydrogen-helium plasma measured by Mijatović *et al.* [27] with an electron density range of $(0.25-0.50)\times10^{22}$ m^{-3}, electron temperatures of $(1.93-2.36)\times10^4$ K, and gas temperatures of $(0.5-1.2)\times10^4$ K—the latter are measured from the Doppler broadening of He I line profiles, (iii) theoretical results by Gigosos *et al.* [23,75], covering a density range of $(0.25-249)\times10^{22}$ m^{-3} and a temperature range of $(1.93-6.34)\times10^4$ K, (iv) the measured values of Pérez *et al.* [5] in the plasma density range of $(1-6)\times10^{22}$ m^{-3} and temperature interval of $(0.8-3)\times10^4$ K with a mean value of 2×10^4 K, and (v) theoretical values from Griem's approach [52], reported by Pérez *et al.* [5]. Good agreement between our results and other investigations is found. Again, the width shows some discrepancy at low densities. As before, this might be due to the lack of ion dynamics in our approach. The calculations in Figs. 7 and 8 with Doppler broadening are shown as well.

In order to compare different theoretical approaches, the ratio of the experimental width to the theoretical one is considered. In this comparison, the width of the experiment performed by Milosavljević and Djeniže [32] is used as a reference. The measured electron densities and temperatures were in the range of $(4.4-8.2)\times10^{22}$ m^{-3} and $(1.8-3.3)\times10^4$ K with error bars ±9% and ±10%, respectively. Figure 9 shows the ratio of the experimental Stark width to the theoretical scaling data of Griem [52], BCW [49], and DSB [50] as a function of temperature taken from the same Ref. [32]. The ratios between experimental FWHM to various theoretical values show some deviations from unity. Our calculations are also included; lower than Griem's values and agree with the values given according to BCW [49], but they are generally somewhat higher than the measured values.

To assess the importance of different effects, the individual contributions due to electrons and ions are compared

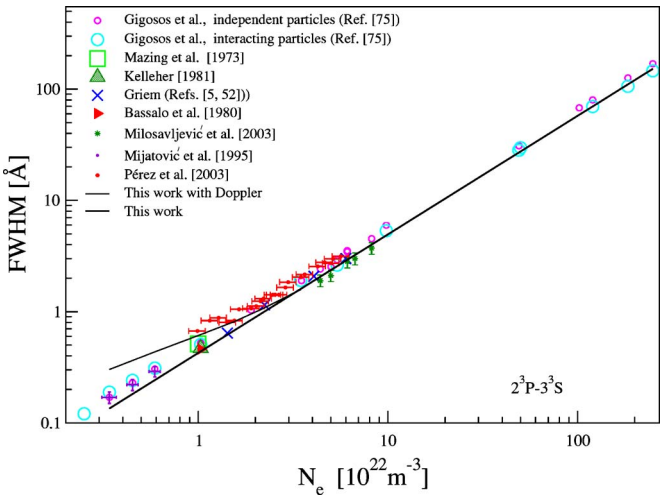

FIG. 8. (Color online) The FWHM of the He I line 7065 Å versus electron density. Comparison is made with available theoretical and experimental data. The electron temperature is taken according to the references [5,27,30,32,52,75–77], see also Sec. III, Table III.

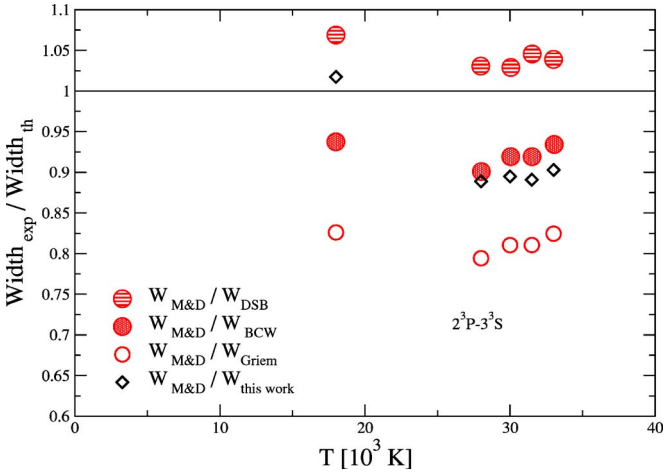

FIG. 9. (Color online) Ratio of the experimental Stark FWHM of the He I line 7065 Å to the various theoretical approaches versus corresponding experimental temperature from Milosavljević and Djeniže [32].

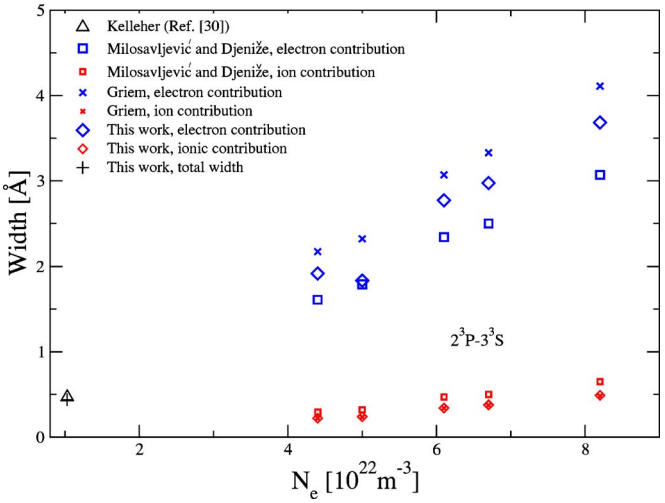

FIG. 11. (Color online) The electronic and ionic width contributions of the He I line 7065 Å versus electron density. Comparison is made with theoretical and experimental data [32].

in Figs. 10 and 11. As can be seen, the ionic contributions to the linewidth is about 19%; in agreement with the values of Griem, and lower than the values given by Milosavljević and Djeniže [32]. Ionic contributions are significantly smaller than electronic contributions. About 13% to 21% of the electronic part is related to the strong collision term. Note also, that the estimated values by Milosavljević and Djeniže [32] give slightly higher results for the ion contributions and smaller values for the electron contributions, but the total width is still lower than theoretical values. Furthermore, the measured value of Kelleher [30] is indicated in Figs. 10 and 11.

Similar calculations are performed for the line 6678 Å. The comparison is shown for FWHM in Figs. 12 and 13 and for the shift in Fig. 14. The experimental FWHM data of Vujicić *et al.* [21] are illustrated in Fig. 12. They have been measured in a laser-produced plasma for electron density $N_e=(0.7-1.7)\times10^{23}$ m^{-3} at an average temperature of $T=3\times10^4$ K, where the validity of the quasi-static approximation is satisfied except in the line center. Also, a forbidden component does not overlap with the isolated one. A comparison was made with the theoretical results of Griem [51,52], Bassalo *et al.* [49], Dimitrijević and Sahal-Bréchot [50] by using Griem's approach for the static ion contributions in Ref. [21]. The agreement of the experimental values, with our best calculations, i.e., including dynamical screening, is better than with the other theoretical approaches. A small discrepancy still remains at high densities, even in case where dynamical screening is included. In Fig. 13, additional data for a larger range of densities are shown: (i) Values obtained by Pérez *et al.* [3] for densities of $(2.0-6.46)\times10^{22}$ m^{-3} and temperatures of $(1.9-4.3)\times10^4$ K, (ii) experimental values by Mijatović *et al.* [27] and Kelleher [30], and (iii) measurement by Milosavljević and Djeniže [31] was

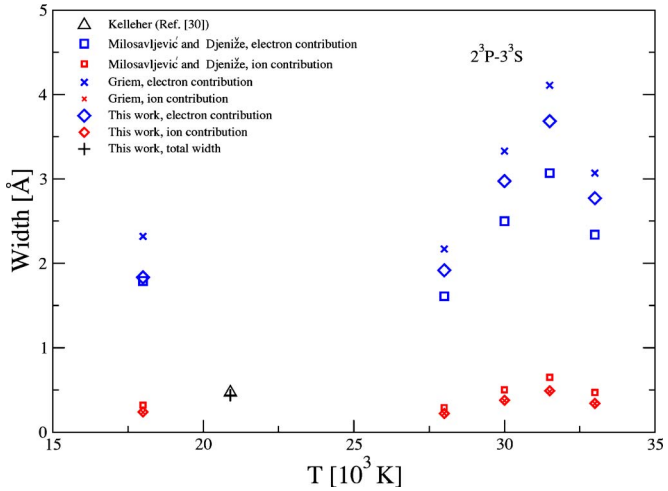

FIG. 10. (Color online) The electronic and ionic width contributions of the He I line 7065 Å as a function of temperature. Comparison is made with theoretical and experimental data [32].

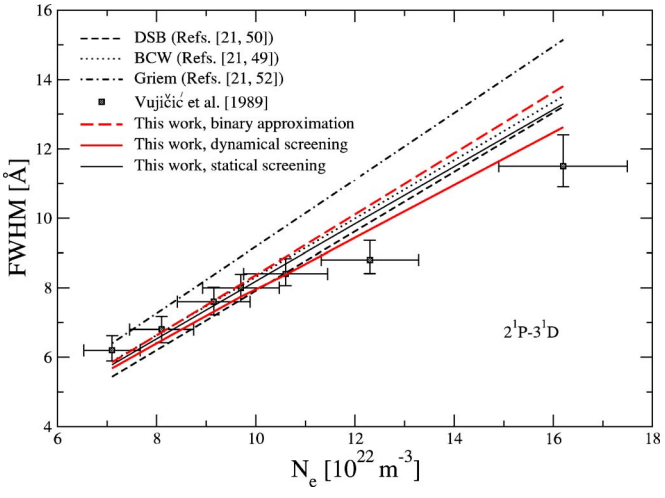

FIG. 12. (Color online) The FWHM of the He I line 6678 Å versus electron density. Comparisons are made with the experimental data of Vujičić *et al.* [21], the calculated theoretical values given in the same reference and our data at an electron temperature 3×10^4 K.

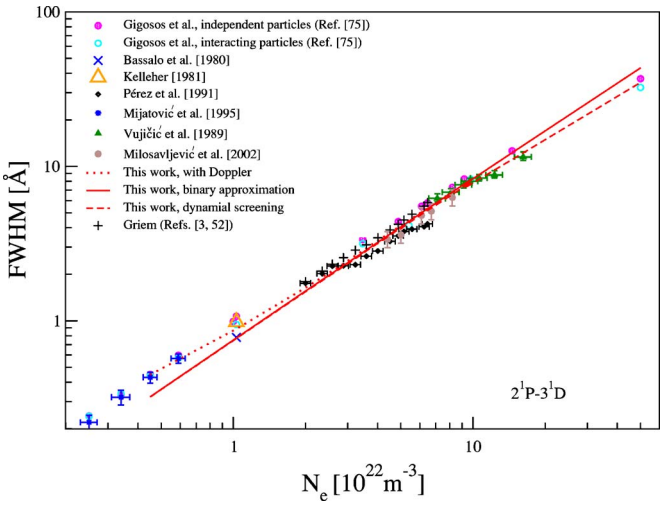

FIG. 13. (Color online) The full width at half maximum of the He I line 6678 Å versus electron density, with and without Doppler broadening, dynamical screening is included. The electron temperature is taken according to the Refs. [3,7,21,27,30,75,76], see also Table III.

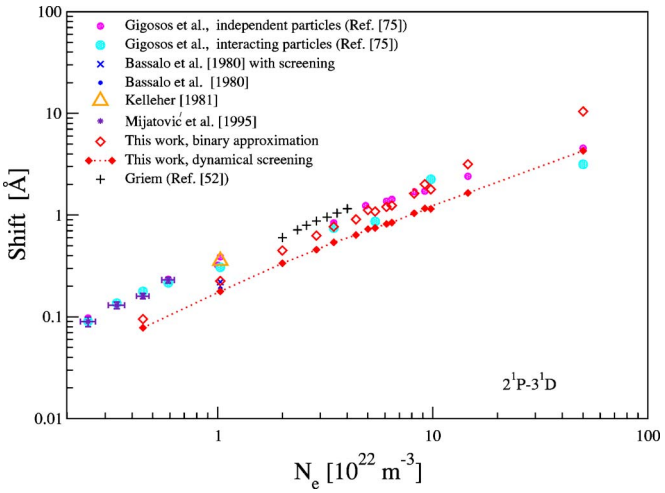

FIG. 14. (Color online) The shift of the He I line 6678 Å versus electron density. Comparison is made with available theoretical and experimental data taking the corresponding electron temperatures [27,30,75,76], see also Table II.

performed at electron densities between $(0.3-8.2)\times10^{22}$ m^{-3} and electron temperatures of $(8-3.3)\times10^4$ K in five different plasma discharge conditions using a linear low-pressure pulsed arc as an optically thin plasma source operated in a helium-nitrogen-oxygen gas mixture. A comparison with the theoretical results by Bassalo *et al.* [76] is given as well. Furthermore, the results by Gigosos *et al.* [23,75] in the density range of $(0.25-50.0)\times10^{22}$ m^{-3} and temperature range of $(1.9-4.2)\times10^4$ K are included.

The Doppler broadening become less important with increasing density, and the width is only due to Stark broadening at high densities. In general, our calculated FWHM results for the given densities and temperatures agree with the other theoretical and experimental values. The theoretical scaling data of Griem for broadening was also given by Pérez *et al.* [3]. We include the line shift in the same manner from Ref. [52]. The estimated values of Griem [52] are systematically higher than our values, especially for the line shift.

As before, the inclusion of dynamical screening reduces the magnitude of both width and shift. It also causes some nonlinear behavior at high densities, see Fig. 14. We find that the shift of this line is more sensitive to plasma screening, as the virtual transitions to neighbored states do not contribute to the line profile if the energy difference is comparable to the plasma frequency [66,78]. The discrepancy between our results and the available data is more pronounced for the shift. For low densities $N_e < 10^{22}$ m^{-3}, the calculated shift is about one-half of the size of the MD data of Gigosos *et al.* [75], while at high densities we overestimate the shift in binary approximation as compared to the MD results. Concerning the high densities, the data by Gigosos *et al.* [75] already indicate the importance of strong coupling effects. Regarding the data point reported by Bassalo *et al.* [76], the discrepancy might be due to neglect of the shift and width in the lower-energy states. Bassalo *et al.* [76] use the Debye radius for the maximum impact parameter and take the reduced matrix elements from the oscillator strength of the transition. In particular, for the line shift, the discrepancies might be related to the somewhat ambiguous definition of the cut-off parameter. In addition, the line might be no longer isolated, or the linear Stark effect might be of importance at high electron densities. Note, that an asymmetric profile of this line was already shown in our previous work [79].

The Stark broadening parameters for the transition 2^1P-4^1S (5048 Å) are given in Table I. Our data, W_{th} and d_{th}, are again compared to calculated values of Bassalo *et al.* [76] and measurements [30,80]. Good agreement is found.

Stark broadening calculations have been also performed for the line 4713 Å. Once again, a linear dependence of the FWHM with the electron density is found in Fig. 15. For this line, Pérez *et al.* [3] have carried out measurements in the temperature range of $(1.9-4.3)\times10^4$ K. In this case, only results for the width with the corresponding theoretical val-

TABLE I. Comparison of the calculated (values without/with screening are given) and experimental results for FWHM and shift are given for line 5048 Å; W_{th} and d_{th} this work; W_{B} and d_{B}, Bassalo *et al.* [76]. The experimental values W_{exp} and d_{exp} have been taken from Table I and II given by Bassalo *et al.*. [76].

N_e (10^{22} m^{-3})	T_e (10^3 K)	W_{B} (Å)	W_{th} (Å)	W_{exp} (Å)	d_{B} (Å)	d_{th} (Å)	d_{exp} (Å)	[Ref. No.]
2.0	18.0	3.10/3.10	3.183/3.179	3.4	1.43/1.35	1.783/1.605	0.9	[80]
1.03	20.9	1.58/1.58	1.623/1.622	1.68	0.75/0.68	0.862/0.788	0.89	[30]

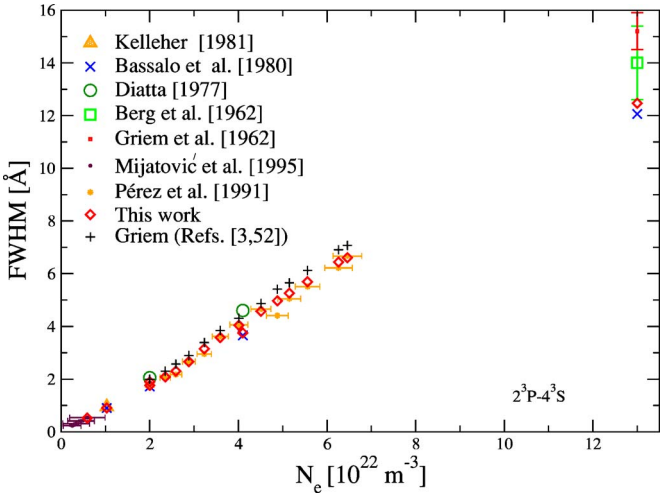

FIG. 15. (Color online) The full width at half maximum of the He I line 4713 Å as a function of electron density. Available theoretical and experimental data are included. The electron temperature is taken according to Refs. [3,27,29,30,76,80], see also Table III.

ues from the Griem approach [3,52] have been reported. Besides the experimental results [27,29,30,80], the theoretical values [29,76] for both width and shift are also shown in Figs. 15 and 16. We notice good agreement between our results and the other data, especially at lower densities. At the highest density, some disagreement is found among the various data. However, at this density, the experimental error bars are also larger.

For the same transition, spectral line profiles have been measured by Milosavljević and Djeniže [31] in the temperature range of $(18-33)\times10^3$ K and electron density of $(4.4-8.2)\times10^{22}$ m^{-3}. From the observed profiles, using a deconvolution procedure, ion static and dynamic broadening parameters were estimated. However, in this case, dynamical ion contributions play no role [31]. The comparison of our results, the experimental data, the theoretical values of

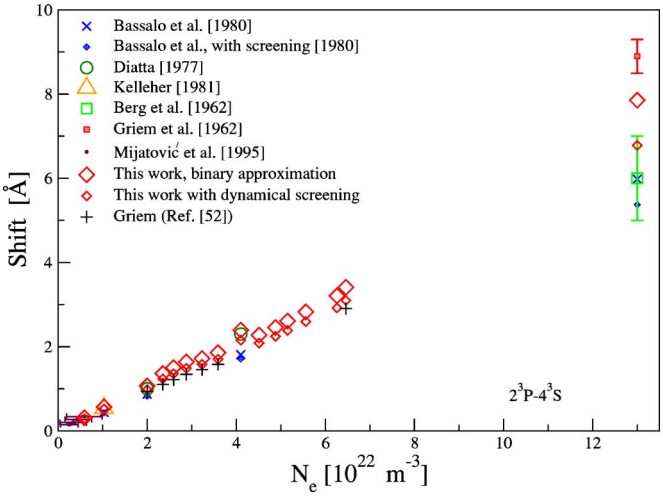

FIG. 16. (Color online) The shift of the He I line 4713 Å as a function of electron density. Comparison is made with previous theoretical and experimental data. The electron temperature is taken according to Refs. [27,29,30,76,80], see also Table II.

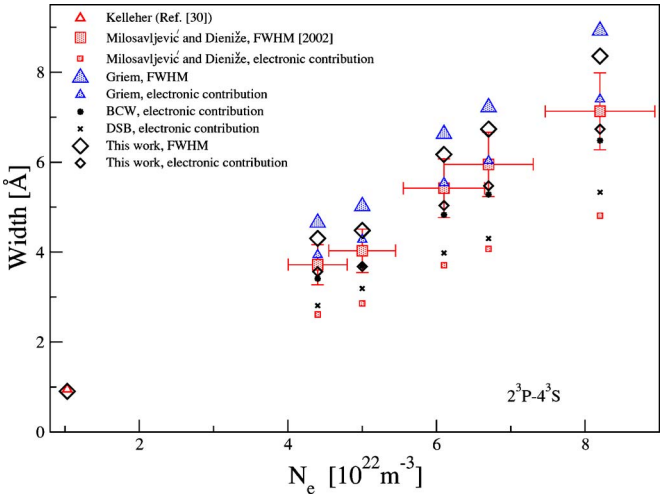

FIG. 17. (Color online) Stark width versus electron density of the He I line 4713 Å. The experimental data of Milosavljević and Djeniže [31], and the theoretical data of Griem [52], BCW [49], and DSB [81] reported from the same Ref. [31], are compared with our calculations.

Griem [51,52], BCW [49], and DSB [81] reported by the same Ref. [31] are presented in Fig. 17. Our electronic contributions lie above BCW [49], the total width is slightly larger than the experimental values but smaller than Griem's approach. Moreover the experimental result of Kelleher [30] is implied.

In order to represent the data more clearly, the values for FWHM and shift obtained in our approach are compared with other theoretical approaches as well as experimental data in Tables II and III, respectively.

As mentioned, the binary collision approximation can be evaluated starting with Eq. (12). The results for the line shift d_1 for line 7065 Å are given in Table IV. Based on the binary collision approximation, the line shift d_2 for static Debye screening can be found by using κ as the lower limit of the q-integration. The contribution of the dynamical screening effect d_3 is obtained by using the full expression for the imaginary part of the inverse dielectric function as given in Eq. (9). The correction due to the static Debye screening leads to reduction of the shift at large values of κ, which correspond to the high electron density and relative low temperature, but it does not influence the width.

In our calculations, the ions have been treated as stationary during the mean time of an electron collision. The static microfield leads to a discrepancy at very low plasma densities, where the motion of ions is more important. The static microfield approach can be improved by using the model microfield method [71,82] or MD simulations [23,72,75]. However, for a nonhydrogenic isolated neutral atomic line, a simple expression can be given, which closely approximates the ion dynamics contribution. In particular, following the unified adiabatic theory, which was independently developed by Griem [52] and by Barnard, Cooper, and Smith (BCS) [83], such an expression can be given in terms of a dynamic ion broadening parameter [27,30–32,40]. This parameter is equal to unity for the measured values of lines 4713 Å and

TABLE II. Comparison of the calculated shift (values without/with screening) d_B by Bassalo *et al.* [76], d_G from MD simulation by Gigosos *et al.* [75] for independent and interacting particles, our calculation d_{th} and the experimental results d_{exp} have been taken from Refs. [4,5,27–30,80].

λ(Å)	$N_e(10^{22}\ \mathrm{m}^{-3})$	$T_e(10^3\ \mathrm{K})$	d_B (Å)	d_G	d_{th} (Å)	d_{exp}(Å)	[Ref. No.]
7281	0.6	4.0	-	-	0.208/0.193	0.16±15%	[28]
	1.03	20.9	0.37/0.36	0.528/0.480	0.438/0.404	0.473	[30]
	3.469	20.0	-	1.66/1.49	1.552/1.42	1.48	[4]
	9.118	20.0	-	4.34/-	4.212/3.793	4.30	[4]
7065	0.45	22.7	-	0.137/0.139	0.122/0.112	0.14	[27]
	1.03	20.9	0.23/0.23	0.327/0.301	0.291/0.265	0.302	[30]
	3.48	20.0	-	1.91/0.93	1.02/0.928	1.07	[5]
	249.0	63.476	-	65.0/52.7	66.25/55.57	-	
6678	1.03	20.9	0.22/0.19	0.389/0.307	0.225/0.178	0.355	[30]
	4.88	42.05	-	1.24/-	0.91/0.66	-	
	6.46	36.45	-	1.43/-	1.242/0.846	-	
	8.2	31.5	-	1.7/-	1.63/1.04	-	
4713	0.59	23.6	-	-	0.31/0.286	0.34±0.015	[27]
	1.03	20.9	0.44/0.43	-	0.569/0.52	0.538	[30]
	2.0	18.0	0.87/0.83	-	1.07/0.982	1.0	[80]
	4.1	20.0	1.81/1.71	-	2.393/2.153	2.3	[80]
	13.0	20.0	5.98/5.37	-	7.853/6.783	6.0±1.0	[29]

5016 Å in Ref. [31]. Therefore, the effect of ion dynamics is negligible for the given electron density and temperature.

IV. CONCLUSIONS

A quantum statistical approach using the technique of thermodynamic Green function is applied to calculate in-medium modifications of spectral lines in dense plasmas. The approach has been used before to hydrogen and hydrogenlike ionic spectral lines [57,63]. In the present work, this approach has been extended to the helium atom, and applied for the electron density range of $(10^{16}-10^{18})\mathrm{cm}^{-3}$ and temperature range of $(1-6)\times 10^4$ K.

TABLE III. Comparison of the calculated FWHM (values without/with screening are given) W_B of Bassalo *et al.* [76], W_G from molecular dynamic simulation by Gigosos *et al.* [75] for independent and interacting particles, our calculation W_{th} and the experimental values W_{exp} are given in Refs. [3–5,27,29–32,80].

λ(Å)	$N_e(10^{22}\ \mathrm{m}^{-3})$	$T_e(10^3\ \mathrm{K})$	W_B (Å)	W_G	W_{th} (Å)	W_{exp} (Å)	[Ref. No.]
7281	1.03	20.9	0.8/0.8	0.929/0.90	0.813/0.813	0.88	[30]
	3.469	20.0		3.20/2.97	2.795/2.794	3.84	[4]
	9.188	20.0		8.43/-	7.602/7.596	9.24	[4]
7065	0.45	22.7		0.23/0.241	0.193/0.193	0.22	[27]
	1.03	20.9	0.46/0.46	0.523/0.507	0.437/0.437	0.47	[30]
	3.48	20.0		1.90/1.91	1.497/1.497	2.04	[5]
	6.1	33.0		3.53/-	3.112/3.112	2.81±0.3372	[32]
	249.0	63.476		169.0/146.0	157.14/156.35		
6678	1.03	20.9	0.78/0.78	1.07/0.946	0.773/0.769	0.98	[30]
	4.88	42.05		4.39/-	3.963/3.895	3.55	[3]
	6.46	36.45		5.79/-	5.316/5.186	4.24	[3]
	8.2	31.5		7.3/-	6.81/6.57	6.28	[31]
4713	0.59	23.6			0.521/0.521	0.54±0.04	[27]
	1.03	20.9	0.90/0.90		0.904/0.904	0.95	[30]
	2.0	18.0	1.72/1.72		1.898/1.898	2.05	[80]
	4.1	20.0	3.66/3.66		3.752/3.75	4.6	[80]
	6.46	36.45			6.614/6.607	6.67	[3]
	13.0	20.0	12.06/12.06		12.496/12.468	14.0±1.4	[29]

TABLE IV. Comparison of the calculated shift values of line (7065 Å) from MD simulation by Gigosos *et al.* [75] for independent and interacting particles d_G, our calculation for binary approximation d_1, by taking Debye screening cut-off parameter d_2 and in the case of dynamical screening d_3 are given.

N_e (10^{22} m^{-3})	T_e(10^3 K)	d_G (Å)	d_1 (Å)	d_2 (Å)	d_3 (Å)
9.8	42.0	3.03/2.59	2.54	2.502	2.352
49.0	44.561	14.7/11.0	13.293	12.818	11.975
50.0	20.0	15.52/12.8	15.557	14.827	13.54
102.0	51.988	29.1/-	27.425	26.229	24.078
120.0	52.104	33.3/29.0	32.558	30.857	28.332
184.0	56.049	49.1/43.4	49.845	46.67	42.453
249.0	63.476	65.0/52.7	66.245	61.496	55.566

Recently, Stark broadening of several helium lines has been observed in various plasma experiments [5,30,32]. An overall good agreement is found by comparing our results with measured values. For higher densities, the behavior of the shift and width of spectral lines becomes nonlinear, see also Fig. 12. A similar behavior is already known from hydrogen [58].

Calculations of helium lines were first performed by Griem *et al.* [51,52]. Other recent calculations of helium line profiles have been performed by Gigosos *et al.* [23,75] based on semiclassical MD simulations for independent, as well as interacting, particles in a nonquenching approximation. In the temperature and density range under consideration, both approaches give results in generally good agreement with our calculations, which are strictly quantum statistical and not restricted to a nonquenching approximation. Moreover, in our calculations, quadrupole contributions are taken into account. The correction due to this contribution increases at high densities. In the region under discussion, all of the considered theories give results for the shift and width of spectral lines which are in reasonable agreement. We expect that our quantum statistical approach can also be used for higher densities to obtain relevant results in this region.

In dense plasmas, where the energy distance between the perturbed and the neighbored perturbing energy levels becomes comparable to the electron plasma frequency, dynamical screening effects are important. Screening reduces the shift especially at a high electron density, analogous to hydrogen [58]. This behavior is shown in Figs. 6 and 12. The linewidth is dominated by the electronic contribution, which is proportional to N_e. This can be seen in Fig. 11.

At high densities, pair-correlation effects are important for the microfield distribution function. They can be derived by an appropriate approach, such as APEX [84,85] or Monte Carlo simulations [24] in the case of strongly coupled plasmas. At low densities ($N_e < 10^{22}$ m^{-3}), ion dynamics correction is required; while at high density, the motion of the ions is not significant [30]. Furthermore, a microscopic description of strong collisions via a partial summation of the corresponding three-particle T-matrix [57] or the close-coupling method by Schöning [70] should be used to avoid artificial cut-off parameters. This is the object of future work.

ACKNOWLEDGMENTS

The authors express appreciation to Professor H. R. Griem for the assistance, and to Professor M. A. Gonzalez for valuable discussions. This work was supported by the Deutsche Forschungsgemeinschaft within Graduiertenkolleg 567, Sonderforschungsbereich 198, and 652.

[1] H. R. Griem, *Plasma Spectroscopy* (McGraw–Hill, New York, 1964).
[2] W. Lochte-Holtgreven, *Plasma Diagnostics* (American Institute of Physics, New York, 1995).
[3] C. Pérez, I. de la Rosa, A. M. de Frutos, and S. Mar, Phys. Rev. A **44**, 6785 (1991).
[4] C. Pérez, J. A. Aparicio, I. de la Rosa, S. Mar, and M. A. Gigosos, Phys. Rev. E **51**, 3764 (1995).
[5] C. Pérez, R. Santamarta, M. I. de la Rosa, and S. Mar, Eur. Phys. J. D **27**, 73 (2003).
[6] W. T. Chiang, D. P. Murphy, Y. G. Chen, and H. R. Griem, Z. Naturforsch. A **32A**, 818 (1977).
[7] V. Milosavljević and S. Djeniže, Astron. Astrophys. **393**, 721 (2002).
[8] A. Beauchamp, F. Wesemael, and P. Bergeron, Astron. J. **108**, 559 (1997).
[9] M. S. Dimitrijević and S. Sahal-Bréchot, Astron. Astrophys. **136**, 289 (1984).
[10] M. S. Dimitrijević, Astron. Astrophys. **112**, 251 (1982).
[11] D. Branch, S. Benetti, D. Kasen, E. Baron, D. J. Jeffery, K. Hatano, R. A. Stathakis, A. V. Filippenko, T. Matheson, A. Pastorello, G. Altavilla, E. Cappellaro, L. Rizzi, M. Turatto, W. Li, D. C. Leonard, and J. C. Shields, Astron. J. **566**, 1005 (2002).
[12] C. Fransson, R. A. Chevalier, A. V. Filippenko, B. Leibundgut, A. J. Barth, R. A. Fesen, R. P. Kirshner, D. C. Leonard, W. Li, P. Lundqvist, J. Sollerman, and S. D. Van Dyk, Astron. J. **572**, 350 (2002).
[13] N. A. Webb, T. Naylor, and R. D. Jeffries, Astron. J. **568**, L45 (2002).

[14] J. A. Harvin, D. R. Gies, W. G. Bagnuolo, Jr., L. R. Penny, and M. L. Thaller, Astron. J. **565**, 1216 (2002).
[15] C. S. Jeffery, J. S. Drilling, P. M. Harrison, U. Heber, and S. Moehler, Astron. Astrophys. **125**, 501 (1997).
[16] C. Rossi, R. F. Viotti, Th. Gäng, G. Bonanno, P. Bruno, A. Cali, R. Cosention, S. Scuderi, M. C. Timpanaro, and S. Desidera, in *Proceedings of the conference "P Cygni 2000, 400 Years of Progress,"* Armagh, 21–23 August 2000. ASP Conference Series Vol. 233, edited by C. Sterken and M. de Groot (2001).
[17] E. L. Robinson, I. I. Ivans, and W. F. Welsh, Astron. J. **565**, 1169 (2002).
[18] J.-C. Gauthier, J.-P. Geindre, C. Goldbach, N. Grandjouan, A.Mazure, and G. Nollez, J. Phys. B **14**, 2099 (1981).
[19] T. Wilhein, D. Altenbernd, U. Teubner, E. Förster, R. Häßner, W. Theobald, and R. Sauerbrey, J. Opt. Soc. Am. B **15**, 1235 (1998).
[20] U. Andiel, K. Eidmann, K. Witte, R. Mancini, and P. Hakel, J. Mod. Opt. **49**, 2615 (2002).
[21] B. T. Vujicić, S. Djurović, and J. Halenka, Z. Phys. D: At., Mol. Clusters **11**, 119 (1989).
[22] B. Ya'akobi, E. V. George, G. Bekefi, and R. J. Hawryluk, J. Phys. B **5**, 1017 (1972).
[23] M. A. Gigosos, M. A. Gonzalez, B. Talin, and A. Calisiti, in *Proceedings of the 17th International Conference on Spectral Line Shapes*, edited by E. Dalimier (Frontier Group, Paris 2004), p. 451.
[24] A. Y. Potekhin, G. Chabrier, and D. Gilles, Phys. Rev. E **65**, 036412 (2002).
[25] N. Konjević, A. Lesage, J. R. Fuhr, and W. L. Wiese, J. Phys. Chem. Ref. Data **31**, 819 (2005).
[26] N. Konjević, A. Lesage, J. R. Fuhr, and W. L. Wiese, J. Phys. Chem. Ref. Data **31**, 819 (2002).
[27] Z. Mijatović, N. Konjević, M. Ivković, and R. Kobilarov, Phys. Rev. E **51**, 4891 (1995).
[28] S. Djeniže, Lj. Skuljan, and R. Konjević, J. Quant. Spectrosc. Radiat. Transf. **54**, 581 (1995).
[29] H. F. Berg, A. W. Ali, R. Lincke, and H. R. Griem, Phys. Rev. **125**, 199 (1962).
[30] D. E. Kelleher, J. Quant. Spectrosc. Radiat. Transf. **25**, 191 (1981).
[31] V. Milosavljević and S. Djeniže, New Astron. **7**, 543 (2002).
[32] V. Milosavljević and S. Djeniže, Eur. Phys. J. D **23**, 385 (2003).
[33] A. Sreckovic, S. Bukvic, and S. Djeniže, Eur. Phys. J. D **30**, 93 (2004).
[34] S. Büscher, S. Glenzer, Th. Wrubel, and H.-J. Kunze, J. Quant. Spectrosc. Radiat. Transf. **54**, 73 (1995).
[35] A. G. Frank, V. P. Gavrilenko, and N. P. Kyrie, in *Proceedings of the 16th of the International Conference on Spectral Line Shapes*, edited by Ch. A. Back (AIP, Melville, New York, 2002) p. 421.
[36] H. G. Adler and A. Piel, J. Quant. Spectrosc. Radiat. Transf. **45**, 11 (1991).
[37] V. Milosavljevic and S. Djeniže, Eur. Phys. J. D **15**, 99 (2001).
[38] D. J. Heading, J. P. Marangos, and D. D. Burgess, J. Phys. B **25**, 4745 (1992).
[39] H. Suemitsu, K. Iwaki, Y. Takemoto, and E. Yoshida, J. Phys. B **23**, 1129 (1990).
[40] R. Kobilarov, N. Konjevic, and M. V. Popovic, Phys. Rev. A **40**, 3871 (1989).
[41] Y. Guimeráns, E. J. Iglesias, D. Mandelbaum, and A. Sánchez, J. Quant. Spectrosc. Radiat. Transf. **42**, 39 (1989).
[42] J. R. Greig and L. A. Jones, Phys. Rev. A **1**, 1261 (1970).
[43] D. D. Burgess and C. J. Cairns, J. Phys. B **4**, 1364 (1971).
[44] J. W. Birkeland, M. E. Bacon, and W. G. Braun, Phys. Rev. A **3**, 354 (1971).
[45] R. N. Morris and J. Cooper, Can. J. Phys. **51**, 1746 (1971).
[46] J. E. Jenkins and D. D. Burgess, J. Phys. B **4**, 1353 (1971).
[47] G. Röpke, T. Seifert, and K. Kilimann, Ann. Phys. (N.Y.) **38**, 381 (1981).
[48] S. Günter, Contrib. Plasma Phys. **29**, 479 (1989).
[49] J. M. Bassalo, M. Cattani, and V. S. Walder, J. Quant. Spectrosc. Radiat. Transf. **28**, 75 (1982).
[50] M. S. Dimitrijević and S. Sahal-Bréchot, J. Quant. Spectrosc. Radiat. Transf. **31**, 301 (1984).
[51] H. R. Griem, M. Baranger, A. C. Kolb, and G. Oertel, Phys. Rev. **125**, 177 (1962).
[52] H. R. Griem, *Spectral Line Broadening by Plasmas* (Academic, New York, 1974).
[53] M. A. Gonzalez (private communication).
[54] A. Brissaud, C. Goldbach, J. Leorat, A. Mazure, and G. Nollez, J. Phys. B **9**, 1147 (1976).
[55] A. Calisti, R. Stamm, and B. Talin, Phys. Rev. A **38**, 4883 (1988).
[56] S. Günter, L. Hitzschke, and G. Röpke, Phys. Rev. A **44**, 6834 (1991).
[57] S. Günter, IPP MPI Report No. 5/67 (unpublished).
[58] S. Böddeker, S. Günter, A. Könies, L. Hitzschke, and H.-J. Kunze, Phys. Rev. E **47**, 2785 (1993).
[59] A. Döhrn, P. Nowack, A. Könies, S. Günter, and V. Helbig, Phys. Rev. E **53**, 6389 (1996).
[60] S. Günter and A. Könies, Phys. Rev. E **55**, 907 (1997).
[61] W. Kraeft, D. Kremp, W. Ebeling, and G. Röpke, *Quantum Statistics of Charged Particle Systems* (Akademie-Verlag, Berlin, 1986).
[62] L. Hitzschke, G. Röpke, T. Seifert, and R. Zimmermann, J. Phys. B **19**, 2443 (1986).
[63] S. Sorge, A. Wierling, G. Röpke, W. Theobald, R. Sauerbrey, and T. Wilhein, J. Phys. B **33**, 2983 (2000).
[64] C. F. Hooper, Jr., Phys. Rev. **165**, 215 (1968).
[65] S. Günter and A. Könies, J. Quant. Spectrosc. Radiat. Transf. **52**, 819 (1994).
[66] L. Hitzschke and S. Günter, J. Quant. Spectrosc. Radiat. Transf. **56**, 423 (1996).
[67] D. R. Bates and A. Damgaard, Philos. Trans. R. Soc. London, Ser. A **242**, 101 (1949).
[68] I. I. Sobelman, *Atomic Spectra and Radiative Transitions* (Springer, Berlin, 1992).
[69] H. R. Griem, Phys. Rev. **128**, 515 (1962).
[70] T. Schöning, J. Phys. B **26**, 899 (1993).
[71] G. Röpke, S. Sorge, and A. Wierling, Contrib. Plasma Phys. **41**, 187 (2001).
[72] S. Sorge, S. Günter, and G. Röpke, J. Phys. B **32**, 675 (1999).
[73] H. A. Bethe and E. E. Salpeter, *Quantum Mechanics of One- and Two-Electron Atoms* (Plenum, New York, 1977).
[74] J. Halenka, Z. Phys. D: At., Mol. Clusters **16**, 1 (1990).
[75] M. A. Gigosos *et al.* (unpublished).
[76] J. M. Bassalo, M. Cattani, and V. S. Walder, Phys. Rev. A **22**, 1194 (1980).

[77] M. A. Mazing and V. A. Selemzin, Sov. Phys. Lebedev. Inst. Rep. **4**, 42 (1973).
[78] G. Röpke, H. Reinholz, C. Neissner, B. Omar, and A. Sengebusch, Contrib. Plasma Phys. **45**, 414 (2005).
[79] B. Omar, A. Wierling, S. Günter, and G. Röpke, in *Proceedings of the 17th International Conference on Spectral Line Shapes*, edited by E. Dalimier (Frontier Group, Paris, 2004), p. 150.
[80] C. S. Diatta, thesis, University d'Orleans, 1977.
[81] M. S. Dimitrijević and S. Sahal-Bréchot, Astron. J. **82**, 519 (1990).
[82] J. Seidel, Z. Naturforsch. A **34A**, 1385 (1979).
[83] J. Barnard, J. Cooper, and E. W. Smith, J. Quant. Spectrosc. Radiat. Transf. **14**, 1025 (1974).
[84] C. A. Iglesias, Phys. Rev. A **27**, 2705 (1983).
[85] C. A. Iglesias, J. L. Lebowitz, and D. MacGowan, Phys. Rev. A **28**, 1667 (1983).